Impact on EoR Power Spectrum of Calibration of Ionospheric Parameters for SKA1-LOW

Cathryn Trott
International Centre for Radio Astronomy Research, Curtin University

October 5, 2015

Abstract

In this brief note I compare different proposed SKA1-LOW array layouts for the task of performing an Epoch of Reionisation (EoR) power spectrum analysis, in the context of the ability of the data to estimate ionospheric phase parameters. I outline an approach that computes the Fisher Information of the amplitude of parameters describing an ionospheric model that are contained within the extended baseline data towards high SNR calibration sources. Distributed pierce points through the ionosphere sample the distortion pattern adequately and allow for precise estimation of model parameters. The parameter uncertainties are then propagated through a statistical model for the distribution of point sources across the field-of-view to compute the covariance of the data due to an imprecisely-estimated ionosphere. This data covariance is then propagated into the two-dimensional power spectrum, as a metric used for EoR estimation, to determine the impact in wavenumber space. Despite yielding the same number of pierce points towards the ionosphere with redundant information (same pierce points), the superstation design provides additional sensitivity, yielding more precise calibration and consequently less impact on the EoR power spectrum at 50 MHz and 150 MHz. At higher frequencies (250 MHz), the reduced field-of-view yields calibration improvement for arrays that sample the ionospheric pierce points more completely, with less calibrators available. This note does not make any assessments of the relative science capabilities of the arrays (e.g. reduced sensitivity to EoR power spectrum due to relocation of core sensitivity to non-core sensitivity).

Introduction

Plasma within the upper layers of the Earth's atmosphere, including the ionosphere, distort plane-wave wavefronts from point sources in the far field. This distortion introduces delays in arrival of the wavefront to different sampled locations on the ground (i.e., dipoles and stations), yielding an additional phase term in the measured visibilities and a consequent apparent shift in the location of a source. For distributed arrays, such as SKA1-LOW, the pierce points through the ionosphere toward a given source from different stations sample differing ionospheric conditions, making instrument calibration difficult. One way to mitigate this is to have a parametric model for the ionosphere, and fit to this model. With sufficient distribution of pierce points, and reduced number of parameters to estimate, the model may be fitted with some precision by using bright calibrator sources within the field-of-view. The remaining imprecision in the model adds uncertainty to the science-quality data, which may impact the ability to achieve some scientific goals. Furthermore, the calibration imprecision may lead to correlated errors in the data, which manifest in a non-uniform way in the data products.

The EoR power spectrum is a metric used to perform statistical estimation of the EoR signal, and computes the power (variance) as a function of spatial scale. Additional correlated phase

errors in calibrated visibilities may lead to structure in the power spectrum. This work aims to determine the impact of these correlated calibration uncertainties on the EoR power spectrum, for different frequencies and potential design layouts for SKA1-LOW.

Approach

We compute the precision with which an optimal, unbiased estimation procedure would estimate the parameters of the ionospheric model, using the Fisher Information and Cramer-Rao Bound, based on data accumulated in 10 seconds over a 10 MHz bandwidth. These data are dual-polarisation visibilities obtained from baselines formed via cross-correlation of all stations, where the core is treated as a single station. These parameter uncertainties are then propagated into a model for the visibilities measured from sources distributed across the field-of-view, including a component of the visibility phase that encodes the position shifts due to the ionosphere. The uncertainties are then further propagated into the two-dimensional power spectrum $(k_\perp, k_\parallel)$. We start by defining the ionospheric model, and then describe how the ionosphere alters visibilities.

Ionospheric model

The phase induced by the ionosphere is modelled with a cosine basis function set at frequency ν, such that:

$$\psi(\theta_x, \theta_y; \nu) = \sum_i \alpha_i(\nu) \cos(\theta_x k_i), \tag{1}$$

where k_i describe the angular wavenumbers and α_i are the amplitudes, at Cartesian angles θ_x, θ_y. The model is based on the observations from Loi et al. (2015) at the Murchison Radio Observatory, which measured position offsets with a sinusoidal basis of wavelength $\sim$5 degrees of amplitude 5–10 arcseconds at 150 MHz. These are the observations upon which we base the model used in this work. The amplitude scales with the square of frequency, such that: $\alpha(\nu) = \alpha(\nu_0)(\nu/\nu_0)^{-2}$.

The individual stations pierce the ionosphere in the near-field at an angle θ that depends on the calibrator source position and the station location on the ground:

$$\begin{aligned} \theta_x &= x_j + h\tan(l) \\ \theta_y &= y_j + h\tan(m), \end{aligned} \tag{2}$$

where x_j, y_j is the ground location of station j, h is the ionospheric height (400 km), and l, m are the direction cosines for the calibrator source.

Measurements

The visibilities are measured by forming baselines between the stations. For a baseline formed from stations j and k at frequency ν, the visibility is:

$$V_{jk}(l,m) = \int dS S \frac{dN}{dS} \iint dl dm B(l,m;\nu) \exp(-2\pi i(ul+vm)) \exp(-2\pi i \psi(\theta_x, \theta_y)), \tag{3}$$

where dN/dS is the number density of sources per unit flux density and sky area. We use the model of Intema et al. (2011), observed at 150 MHz.

For the calibration stage, we assume that sources with flux densities $> 5\sigma$ over 10 seconds and 10 MHz (where σ encodes the thermal and confusion noise) are available to be used for pierce points for sampling the ionospheric phase term.

Fisher Information

We compute the Fisher Information, which for iid Gaussian-distributed data, and parameters ϕ_i, ϕ_j is given by:

$$I_{\phi_i,\phi_j} = \sum_{i=1}^{N} \frac{2}{\sigma^2} \left(\frac{\partial V^\dagger}{\partial \phi_i} \frac{\partial V}{\partial \phi_j} \right). \quad (4)$$

The set of these quantities forms a matrix (the Fisher Information Matrix - FIM). Inverting the FIM and taking the square-root of the diagonal components yields the Cramer-Rao Bounds (CRBs) on the parameter estimates for an optimal, unbiased estimator. In this work, the parameters, ϕ are the amplitudes of the cosine basis functions describing the ionosphere, α. We jointly estimate 50 parameters, with wavenumbers, $k = 4n + 8\,\mathrm{rad}^{-1}$, corresponding to angular scales ranging from 0.4–11 degrees.

Error propagation

The CRBs (their squares; the variances) are propagated into the visibilities (Equation 3) measured across the array from all stations and for a full sky model, based on the statistical distribution of Intema et al. (2011). This then yields a covariance matrix for each visibility, with correlations between frequency channels. These covariances are then propagated further into a statistical model for the data distribution as function of frequency and angular wavenumber (u, v). The covariances here are between frequency channels, because the ionospheric calibration uncertainties impact the signal from sources in the sky, which, as continuum sources, have strong spectral correlations.

Arrays considered

We consider seven array configurations, where the core is treated as a single station (or superstation in one array), and the long baselines provide the fundamental pierce point sampling of the ionosphere. The arrays include the spiral SKA Baseline design ('Baseline45'), five semi-random designs proposed by the Architecture Group led by Tim Cornwell (April 2015), and one recent superstation design proposed by the Office ('Spiral94'). The use of 6 stations within each superstation increases the number of baselines by a factor of 36 between two superstations, improving estimation precision by a factor of $\sqrt{36} = 6$. All stations have 35 m diameter, except Spiral94, which has 33 m. Table 1 defines these arrays. Figure 1 displays the non-core station

Name	Total stations	Non-core stations
Baseline45	512	45
Random11	512	11
Random21	512	21
Random31	512	31
Random41	512	41
Random51	512	51
Spiral94	564	6*55=330

Table 1: Names of arrays used in this document, their total number of stations and the number of non-core stations. Total stations used in this work include all non-core stations and the core (treated as a single station). 'Spiral94' comprises 55 superstations consisting each of a central 33 m station surrounded by 5 33 m stations in a closely-packed configuration.

array configurations.

Results

Table 2 lists the precision with which the amplitude of the wavemode with length 4.5 degrees can be estimated, while simultaneously estimating all 50 amplitudes, for each array and each frequency. Addition of stations outside of the core generally leads to improved estimation precision,

Name	Frequency	Num. cals.	Amplitude	Precision
Baseline45	50 MHz	44	0.27 rad	3.9×10^{-5}
Baseline45	150 MHz	67	0.03 rad	3.0×10^{-5}
Baseline45	250 MHz	31	0.01 rad	3.0×10^{-4}
Random11	50 MHz	44	0.27 rad	5.5×10^{-4}
Random11	150 MHz	67	0.03 rad	2.2×10^{-4}
Random11	250 MHz	31	0.01 rad	1.2×10^{-3}
Random21	50 MHz	44	0.27 rad	8.5×10^{-5}
Random21	150 MHz	67	0.03 rad	2.9×10^{-5}
Random21	250 MHz	31	0.01 rad	2.2×10^{-4}
Random31	50 MHz	44	0.27 rad	5.6×10^{-5}
Random31	150 MHz	67	0.03 rad	2.1×10^{-5}
Random31	250 MHz	31	0.01 rad	8.0×10^{-5}
Random41	50 MHz	44	0.27 rad	3.7×10^{-5}
Random41	150 MHz	67	0.03 rad	1.3×10^{-5}
Random41	250 MHz	31	0.01 rad	1.0×10^{-4}
Random51	50 MHz	44	0.27 rad	2.7×10^{-5}
Random51	150 MHz	67	0.03 rad	8.3×10^{-6}
Random51	250 MHz	31	0.01 rad	3.8×10^{-5}
Spiral94	50 MHz	44	0.27 rad	6.0×10^{-6}
Spiral94	150 MHz	67	0.03 rad	4.0×10^{-6}
Spiral94	250 MHz	31	0.01 rad	5.0×10^{-5}

Table 2: Names of arrays, central observing frequency, number of 5σ calibrators available in 10 seconds, amplitude value and precision of estimating the ionospheric value.

as does the extra collecting area of the superstations.

These uncertainties are then propagated into the 2D power spectrum. Figure 2 displays the 50 MHz and 150 MHz power spectra for a selection of the configurations (Random11, Random21, Random51, Baseline45, Spiral94). Figure 3 displays the signal-to-noise ratio (SNR) at 150 MHz of a simple cosmological signal model power spectrum to the calibration error power, for each of six arrays (Random11, Random21, Random41, Baseline45, Spiral94). Aside from the arrays with the fewest non-core stations, the SNR exceeds unity by at least two orders of magnitude across most of the parameter space. Again, the superstation design of Spiral94 provides the precision to calibrate the ionosphere well via the additional sensitivity outside of the core.

Finally, the power at 250 MHz can be computed (Figure 4). Here, the system temperature is much lower than at lower frequencies, but this is balanced by the reduced effective area of the stations. The reduced field-of-view constrains the number of calibrators available. Therefore the sensitivity improvement of the Spiral94 array is not sufficient to balance the lower density of ionospheric pierce points, compared with Random51. Hence, at high frequencies, additional distribution of pierce points yields improved calibration compared with additional sensitivity at

redundant pierce points. Of course, this balance also depends on the amount of data used to calibrate the array.

Summary

Distributed baselines outside of the core of SKA1-LOW yields an adequate sampling of the ionospheric phase screen to allow calibration of the array by use of high SNR point source calibrators. The additional collecting area of the Spiral94 superstation array design yields additional measurements (baselines) with which to sample the ionosphere (albeit at the same pierce point locations), allowing more precise calibration of the point source locations, and therefore more precise array calibration at low frequencies (50 MHz, 150 MHz). At 250 MHz, additional distribution of pierce points yields improved calibration compared with additional sensitivity at redundant pierce points. Given that EoR science is principally concerned with the 50–200 MHz band, the additional sensitivity of the superstations yields improved calibratability.

References

Intema, H T, van Weeren, R J, ,Röttgering, H J A and Lal, D V 2011 A&A **535**, A38.
Loi, S T. et al. 2015 MNRAS, **453**, 2731.

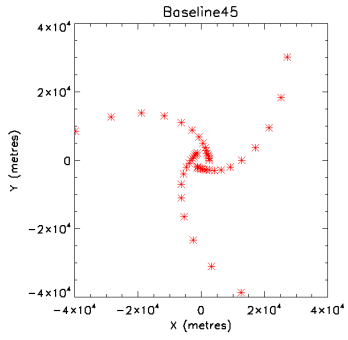

(a) Baseline45

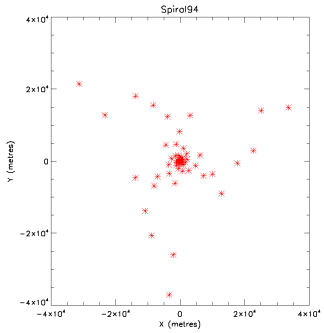

(b) Spiral94 (each asterisk denotes a superstation)

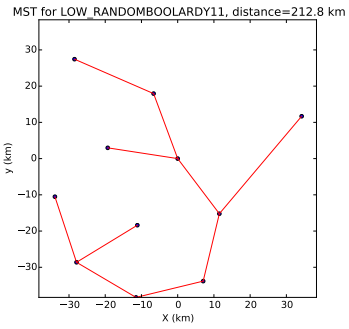

(c) Random11

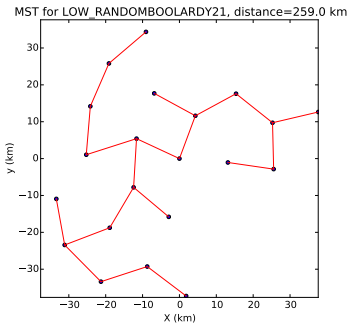

(d) Random21

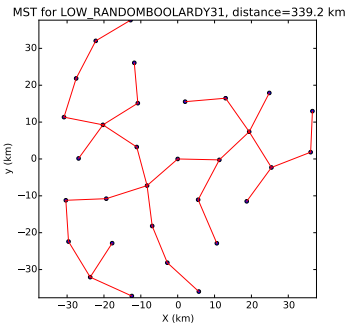

(e) Random31

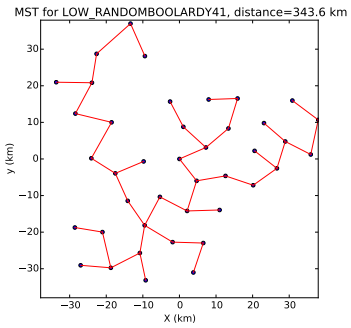

(f) Random41

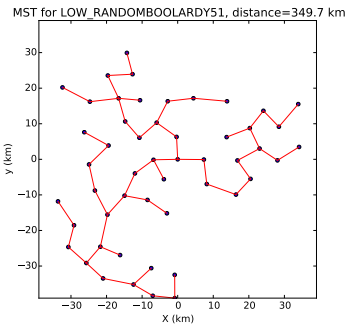

(g) Random51

Figure 1: Arrays considered in this work. Only long (non-core) baselines are shown. The Spiral94 array asterisks denote superstations of 6 33 m stations.

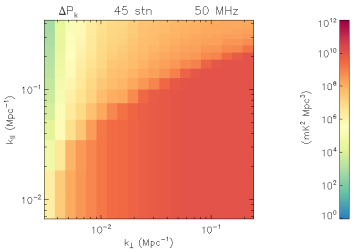

(a) Baseline45 50 MHz

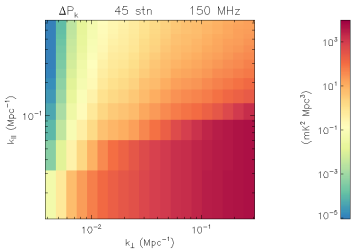

(b) Baseline45 150 MHz

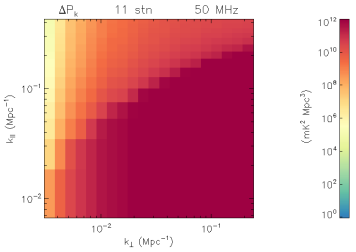

(c) Random11 50 MHz

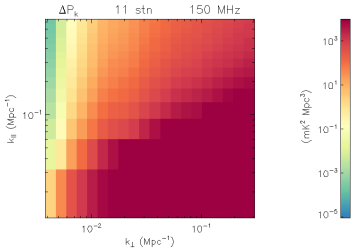

(d) Random11 150 MHz

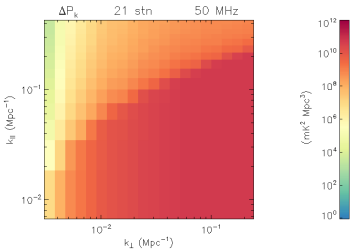

(e) Random21 50 MHz

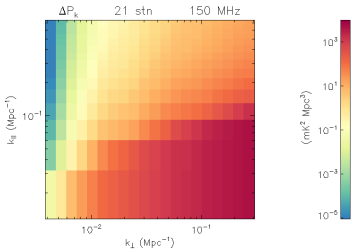

(f) Random21 150 MHz

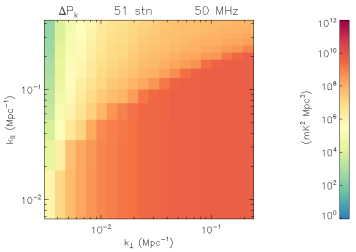

(g) Random51 50 MHz

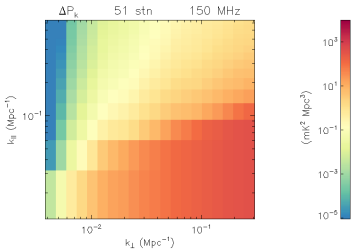

(h) Random51 150 MHz

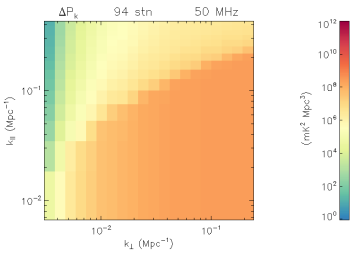

(i) Spiral94 50 MHz

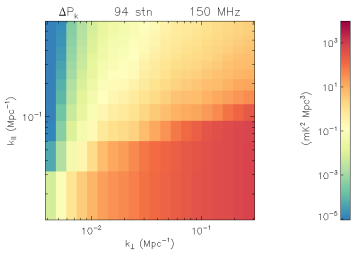

(j) Spiral94 150 MHz

Figure 2: Power introduced by imprecise ionospheric calibration of point sources.

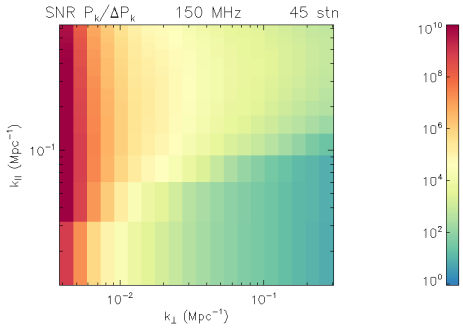

(a) Baseline45

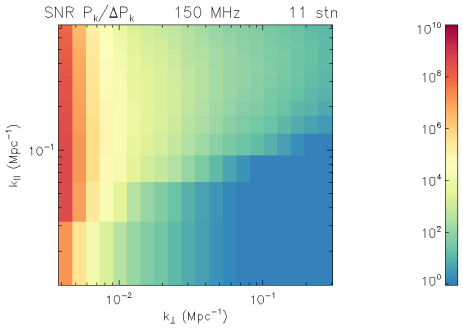

(b) Random11

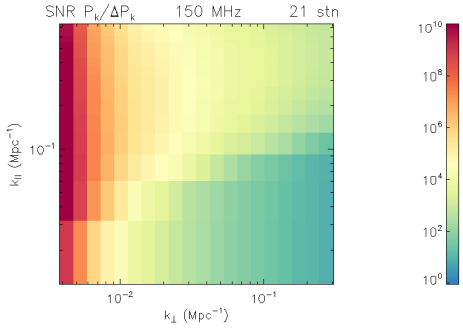

(c) Random21

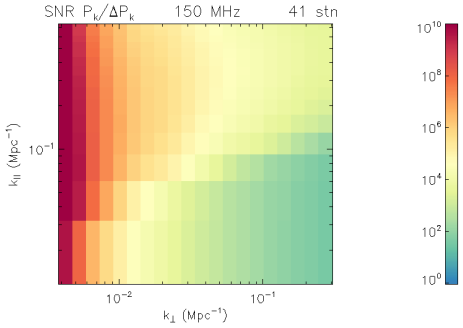

(d) Random41

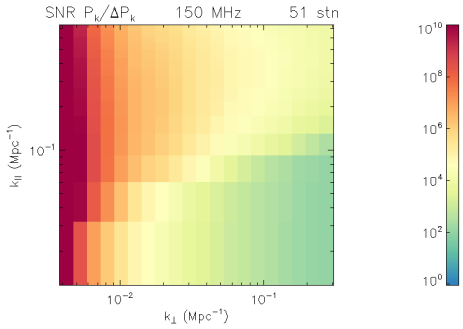

(e) Random51

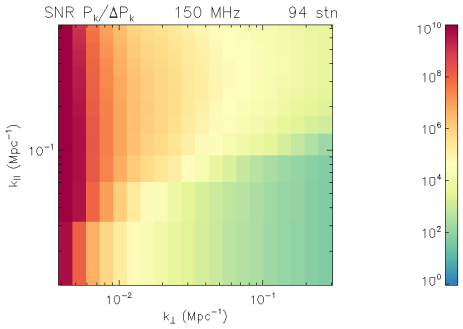

(f) Spiral94

Figure 3: SNR of cosmological signal to errors introduced by imprecise ionospheric calibration.

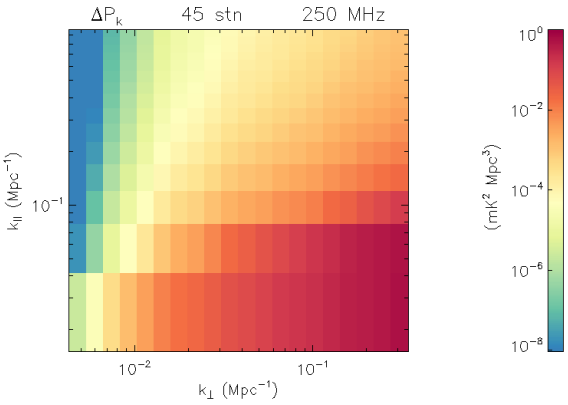

(a) Baseline45

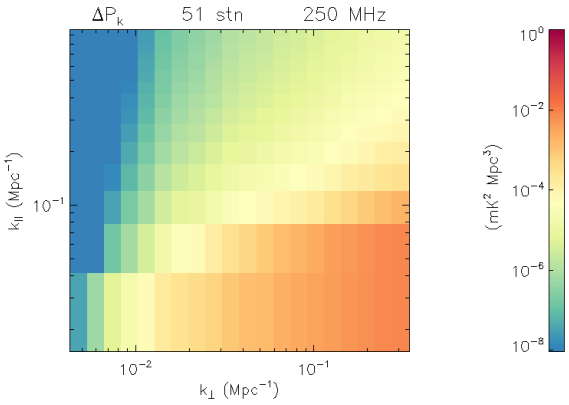

(b) Random51

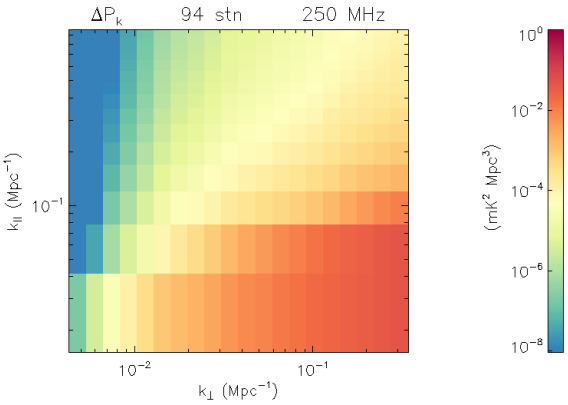

(c) Spiral94

Figure 4: Calibration error power at 250 MHz. The reduced field-of-view at these frequencies yields less improvement from extra sensitivity versus additional pierce points available in the Random51 array.